

Direct Observation of the Translational Immobilization of Water Molecules Under Nanoscale Confinement

Alec A. Beaton¹ and John M. Franck¹

¹*Department of Chemistry, Syracuse University, Syracuse, NY 13210, USA**

(Dated: Tuesday 29th October, 2024)

Overhauser Dynamic Nuclear Polarization (ODNP) detects an experimental measurable associated directly with translational motion of water at the nanoscale, a quantity that few other methods can detect. This study offers a unique insight into the translational diffusion of water inside reverse micelles (RMs). It finds that simply adjusting the “water loading” (w_0 , *i.e.* the mole ratio of surfactant to water) to tune the size of the RMs achieves a near-continuous tuning of the translational diffusion of water. Furthermore, (1) the dynamics of water molecules in the core of relatively large RMs ($w_0 = 10$, diameter of water nanopool ≈ 3.5 nm) diffuse only as fast as those on the surface of a lipid bilayer and (2) surprisingly, translational diffusion slows to a near-stop for RMs that are small, but that still contain hundreds of water molecules in their core. Extrapolation to larger sized water pools implies that in order to recover bulk-like translational dynamics, tens of thousands of water molecules are required. The data from the small RMs also represent a breakthrough as the first example where a spin probe that is completely exposed to water (as opposed to buried inside a macromolecule) observes dramatic slowing of the translational diffusion.

Introduction

Polymer pores, pockets of proteins, and solid-phase meso- and nano-porous systems can all confine water, dramatically altering its properties [1–5] and, therefore, how it contributes to and drives chemistry [6–10]. Reverse micelles (RMs) are an important model system for understanding confined water: one of only a few systems where the size of enclosure can be changed almost continuously without changing the chemical identity of the enclosing structure [3, 11–15]. Previous measurements of RM dynamics include infrared spectroscopy [16] Quasi-Elastic Neutron Scattering (QENS) coupled with molecular dynamics (MD) simulations [17], Dynamic Stokes Shift (DSS) [18–20], pump-probe spectroscopy of infrared (IR)-active probe molecules [21, 22], deuterium or ¹⁷O Nuclear Magnetic Resonance (NMR) [23–25], and dielectric spectroscopy [26]. All tend to indicate reduced mobility of the confined water, but it can be difficult to experimentally isolate the translational diffusion of the confined water; furthermore, especially when the motion is slow, distinguishing the motion of the water from that of the RM can prove challenging. Isolating the translational motion of confined water is crucial, since it is believed to be both decoupled from other motions [27], as well as essential, *e.g.*, to the association of macromolecules and the domain motion of proteins [28, 29], or to explaining important transport properties in energy-relevant materials [30].

Overhauser Dynamic Nuclear Polarization (ODNP) reports specifically on the translational motion of water molecules in the vicinity of a specially placed electron spin probe (SP) – a small molecule or moiety containing a stable unpaired electron spin (typically a nitroxide). Specifically, sufficiently fast translation of the wa-

ter relative to the SP excites a transition that, combined with saturation of the SP Electron Spin Resonance (ESR) transition, leads to NMR signal inversion and enhancement. ODNP reports the rate of this transition as a cross-relaxivity k_σ (with units of cross-relaxation rate per SP concentration) that increases/decreases as the translational mobility of water within 1-1.5 nm of the SP increases/decreases [31–33].

While previous ODNP studies have reported slow water motion at buried sites where relatively few water molecules can access the SP [33–35], none have reported very low translational mobility near SPs that were exposed to significant populations of water molecules. Furthermore, one can imagine a strategy of functionalizing small spin probes designed to associate with particular environments, and then carefully ascertaining their environment with companion measurements. Such a strategy has been relatively underutilized, with many ODNP measurements relying on either covalent attachment to macromolecules or intrinsically present radicals. Past ODNP studies have investigated water dynamics in porous systems [36, 37], and have applied ODNP to RM-encapsulated proteins with a focus of using the combination of ODNP and RMs as a vehicle for signal enhancement of the protein NMR [38]. However, to the authors’ knowledge, no systematic ODNP study has investigated water mobility as a function of confinement lengthscale. The experimental results here dramatically underscore the reality that translational dynamics is a process relying on the collective rearrangement of relatively large masses of water.

SP Localization by Paramagnetic Relaxation Enhancement (PRE)-Relaxation-Ordered Spectroscopy (ROSY)

Basic chemical intuition indicates that the functional groups on small SP molecules should guide the nitroxide into different microenvironments within a heterogeneous

* jmfranck@syr.edu

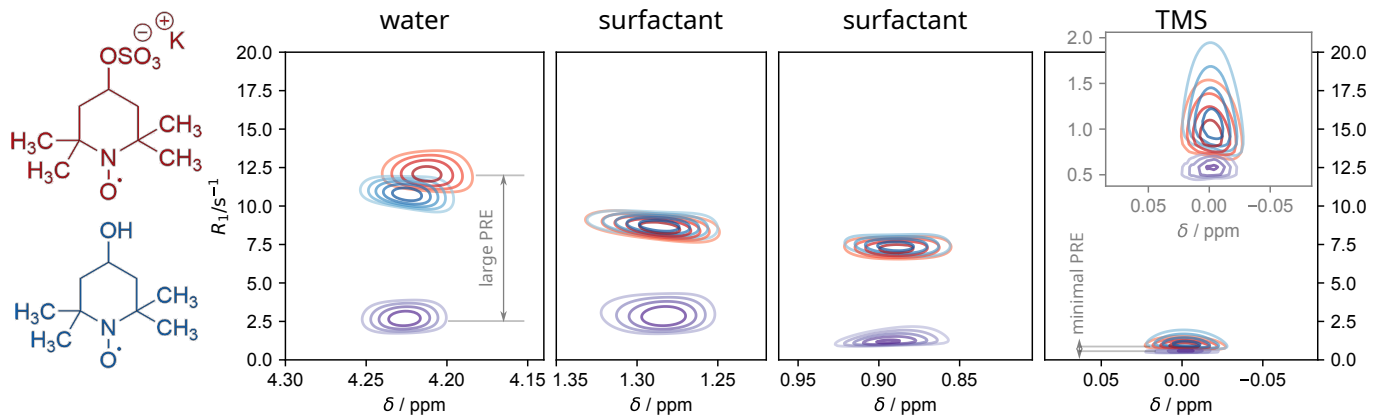


FIG. 1. The water, surfactant (2 strips), and TMS regions of the PRE-ROSY spectra for RM samples that contain water with no SP (purple), *vs.* 70 mM TEMPOL (blue) or 70 mM TEMPO-SO₄ (red). The displacement of the $R_1 = 1/T_1$ in solutions containing spin label (red and blue) relative to the control (purple) is the PRE effect, and indicates the extent to which the species of interest approaches the nitroxide group of the spin label. The inset box (top right, grey border) zooms in on the TMS signal.

system: *e.g.*, the organic *vs.* surfactant *vs.* water regions of the RMs studied here. However, validating the location of the SPs can prove difficult. For example, previous studies reported that zwitterionic SPs have a preference for localization inside the internal water pool of RMs [39]. However, this result relied entirely on inferences from the ESR hyperfine coupling constants, rather than reporting directly on the approach of the nitroxide to specific chemical groups.

Here, we introduce PRE-ROSY for exploring the localization preferences of small SPs. PRE is a well-established NMR technique [40] in which the presence of SPs causes nearby nuclei to relax more rapidly than they would in the absence of the SPs [40]. ROSY spectroscopy can illustrate the distribution of T_1 (*i.e.* longitudinal) NMR relaxation rates ($R_1 = 1/T_1$) both with and without the PRE arising from the incorporated nitroxide SP. The PRE-ROSY experiment (Fig. 1), resolves different compounds according to their chemical shift (along the x -axis), while the displacement along the y -axis indicates how frequently the compound in the mixed-phase system comes close to the SP (Eq. (S5)).

Fig. 1 investigates a RM of $w_0 = 8$, with Aerosol-OT (AOT) surfactant and CCl₄ dispersant. (CCl₄ is both NMR silent and well-documented [13, 17, 26].) It shows RM samples containing water with dissolved TEMPOL (blue) *vs.* TEMPO-SO₄ (red), *vs.* the control (water with no SP, purple). It presents significant evidence that (anionic) TEMPO-SO₄ localizes better to the center of the RM's internal water pool *vs.* (hydrophilic and neutral) TEMPOL. First, the PRE (the displacement along the y -axis away from the purple contour) is significant for both hydroxytempo (blue) and tempo-sulfate (red), indicating that both SPs come into close contact with the water; however, the PRE of the water pool by TEMPO-SO₄ is significantly greater. Second, the TMS peak, which serves as a proxy for the dispersant (which is NMR

silent), experiences a meager PRE effect from both SPs, indicating both tend to stay away from the dispersant; however, the PRE is smaller for TEMPO-SO₄, indicating that it approaches the dispersant (where the TMS resides) less frequently than TEMPOL. Therefore, for studying the water dynamics of the internal water pools, TEMPO-SO₄ was identified as the SP better localized to the center of the water pool.

The SI further discusses the PRE-ROSY (Sec. S3), additional deuterium ROSY (Sec. S4), and ESR [39, 41] (Sec. S4.1) measurements that confirm these results.

ODNP Measurements of Translational Diffusivity

After proper background subtraction of the AOT signal (Fig. S1), Fig. 2a shows the ODNP enhancements for the four different w_0 RMs; where enhancements, $E(p)$, are the ratio of NMR signal with resonant microwaves, and therefore ODNP, *vs.* without. The lowest water loading (blue, $w_0 = 1$) shows only enough ODNP to slightly reduce the NMR signal, and not even enough to invert it. This is consistent with a water matrix whose translational motion is dramatically restricted. The increasingly greater enhancements at increasing w_0 indicate that the larger size of the enclosed water pools enables faster translational diffusion of the water molecules. Overall, it is surprising that the ODNP turns on and almost completely off as the size of the water pool is scaled.

In order to directly relate to translational diffusion, following established analyses [33] (Eq. (S1)), the enhancements are subtracted from 1 and divided by the NMR relaxation times, SP concentration, and a standard set of physical constants to give Fig. 2b. These datapoints, in turn, are fit to an asymptotic microwave power dependence (to model the saturation of the ESR transition, Eq. (S2)) to yield the cross-relaxivity or k_σ of each sample: Table I. The translational retardation factor, $k_{\sigma,bulk}/k_\sigma$, in the second column indicates the slowness/retardation of the translational water diffusion

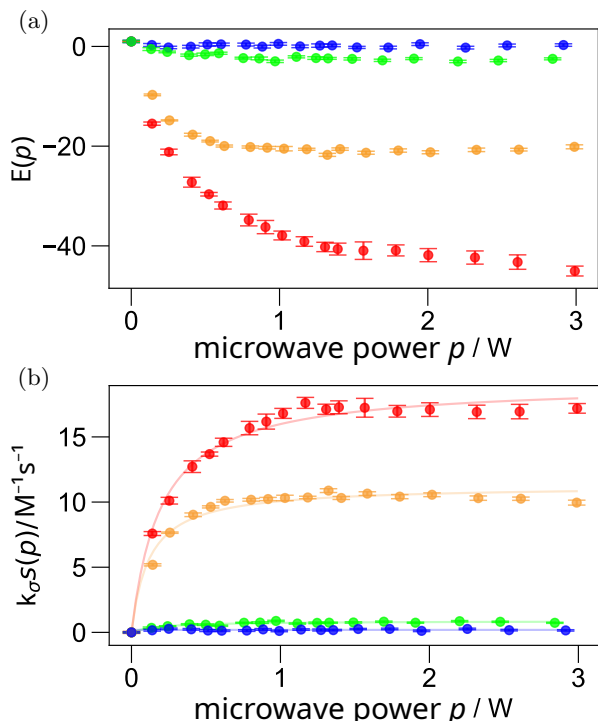


FIG. 2. (a) NMR signal enhancement, as a function of ESR-resonant microwave power, for the AOT/ CCl_4 RMs for $w_0 = 1$ (blue), 5 (green), 7.4 (orange), and 10 (red). Each has been corrected for the corresponding enhancement of the AOT. Dividing out the NMR T_1 relaxation times and several constants (Eq. (S1)) yields the product of the ESR saturation factor and the desired cross-relaxation rate k_σ , which is the asymptotic limit of the fit curve in (b), and which directly indicates substantial variation of the translational motion with w_0 .

w_0	$k_\sigma / M^{-1} s^{-1}$	$k_{\sigma, \text{bulk}} / k_\sigma$	$k_{\text{low}} / k_{\text{low, bulk}}$
1	0.19	320	> 0.81
5	0.87	68	> 0.84
7.4	10.6	8.4	> 0.99
10	19.1	5.0	0.99

TABLE I. Values for k_σ and k_{low} determined for different RM samples, with $k_{\sigma, \text{bulk}} = 95.4 \text{ M}^{-1} \text{ s}^{-1}$ and $k_{\text{low, bulk}} = 366 \text{ M}^{-1} \text{ s}^{-1}$ [33].

relative to bulk [32, 33, 42] and spans two orders of magnitude as the size of the RM is altered.

The translational diffusion of water inside the RM reduces to essentially non-existent levels in the smallest water pools (k_σ 320 \times smaller than in bulk, indicating correspondingly slower water motion). This supports a view that translational motion of water is a collective process that requires hundreds of water molecules in order to achieve standard rates of diffusion [11, 43]. At very small water loadings, the reduced number of water molecules do not provide a sufficiently large number of hydrogen-bonding configurations (microstates) that can

be traversed in order to activate translational motion. As the water pool grows in size, more water molecules are present to enable a larger number of hydrogen bonding configurations, thus enabling faster translational diffusion.

At the highest w_0 studied here, the water still moves less rapidly than in the bulk. Notably, these measurements can be compared against water in the hydration layers of macromolecules dissolved in bulk water solution [33, 44], and a value of $k_{\sigma, \text{bulk}} / k_\sigma \approx 5$ indicates that the water moves at rates comparable to the hydration water coating the surface of a lipid bilayer [44]. At the highest water loading here, $w_0 = 10$, the diameter of the water pool should be about 3.5 nm [45]. (The value of k_{low} , Eq. (S3), for $w_0 = 10$ also matches k_{low} at the surface of a lipid bilayer [33, 44].) However, unlike the lipid bilayer measurements that employ a SP covalently bonded to the surface of the lipid bilayer [44], the spin label in the current measurements spends most of its time near the middle of the enclosed water pool. Specifically, note that Fig. 1 shows a significantly greater PRE of the water *vs.* surfactant, thus indicating the SP spends little time near the surfactant.

Furthermore, k_{low} (determined from the self-relaxivity, with the fast-motional contribution subtracted out: Eq. (S3)), samples the dynamics of water in frequency space at a frequency that is 660 \times smaller than that of k_σ [33]. (~ 660 is the ratio between the ESR and NMR frequencies.) Thus, both fast and slow motions contribute to k_{low} , with the slow motions likely including (or dominated by) rotation of the entire RM. The value of k_{low} serves as a control to see whether or not the water molecules are still experiencing dipolar coupling with the SP. In all cases, the values of k_{low} in Table I demonstrate good interaction of the water molecules with the SP. Thus, k_σ falls off at low w_0 not because of any lack of magnetic dipolar coupling between the SP and water, but because the translational motions of the water are simply not faster than the hundreds-of-picosecond timescales needed to achieve significant excitation of the cross-relaxation (k_σ) transition [31–33, 46].

Overall, these measurements provide greater insight into water that occurs naturally in confinement, ranging from pockets on the surface of proteins, to inside cellular vesicles (*e.g.* lysosomes and endosomes), to the pores of synthetic mesoporous systems, and could pave the way for improved understanding of the function of these systems. Fig. 3 emphasizes the near-total shut-down of translational diffusion for water pools of diameter ~ 1.75 nm. As previously noted, for the small water pools present at low water loadings, the dearth of different hydrogen bonding rearrangements possible leads to a slowdown in the translational motion of the water molecules. However, the lengthscale at which this effect sets in is surprising: a RM of $w_0 = 4.5 - 5$ encapsulates hundreds of water molecules [47, 48].

Linear extrapolation (Fig. 3) to $k_\sigma / k_{\sigma, \text{bulk}} = 1$ indicates that a water loading of $w_0 = 31$ would be required

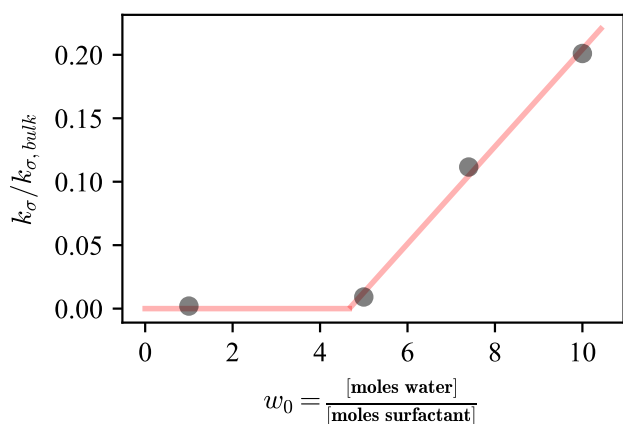


FIG. 3. The variation of translational mobility, as quantified by the ODNP cross-relaxivity (normalized against the cross-relaxivity of a small spin label dissolved in bulk water $k_{\sigma, \text{bulk}}$) as a function of the degree of confinement—given here by the water loading w_0 . Note that the diameter of the water pool can be approximated by $w_0 \times 0.35$ nm.

before the water in the center of the pool diffused at rates approaching those seen in bulk solution. Again, the relatively large size of the water pool required proves surprising, as RMs of this lengthscale contains an aqueous core ~ 11 nm in diameter, containing tens of thousands of water molecules.

It is worth noting that these experiments were initially designed with the intention of determining the thickness of the hydration layer from the perspective of ODNP by looking for a moderate change in k_σ with the size of the reverse micelle. However, they ended up highlighting how dramatically the translational mobility depends on the level of confinement. As such, this study also opens up the pathway to future measurements where RMs serve to relate measurements of dynamics to a lengthscale of confinement, in particular for ODNP measurements run at lower resonance frequencies that can ostensibly detect the dynamics of the slower water inside severely confined (*i.e.* small) RMs. It also clearly points to future measurements where PRE-ROSY can verify the location of a spin probe inside a small but water-filled pocket of a protein or other macromolecule, while ODNP can elegantly analyze the translational diffusivity within that pocket.

-
- [1] D. Laage, T. Elsaesser, and J. T. Hynes. “Water Dynamics in the Hydration Shells of Biomolecules.” *Chem. Rev.*, 117(16):10694–10725 (2017). doi:10.1021/acs.chemrev.6b00765.
- [2] D. Zhong, S. K. Pal, and A. H. Zewail. “Biological water: A critique.” *Chem. Phys. Lett.*, 503(1-3):1–11 (2011). doi:10.1016/j.cplett.2010.12.077.
- [3] M. Fardis, M. Karagianni, L. Gkoura, and G. Papavasiliou. “Self-Diffusion in Confined Water: A Comparison between the Dynamics of Supercooled Water in Hydrophobic Carbon Nanotubes and Hydrophilic Porous Silica.” *Int. J. Mol. Sci.*, 23(22):14432 (2022). doi:10.3390/ijms232214432.
- [4] F. Persson, P. Söderhjelm, and B. Halle. “How proteins modify water dynamics.” *J. Chem. Phys.*, 148(21):215103 (2018). doi:10.1063/1.5026861.
- [5] Kang Hu and Ryo Shirakashi. “Dynamic Electric Field Alignment Determines the Water Rotational Motion around Protein.” *J. Phys. Chem. B*, 127(6):1376–1384 (2023). PMID: 36749793. doi:10.1021/acs.jpcc.2c07405.
- [6] D. Muñoz-Santiburcio and D. Marx. “Confinement-Controlled Aqueous Chemistry within Nanometric Slit Pores.” *Chem. Rev.*, 121(11):6293–6320 (2021). doi:10.1021/acs.chemrev.0c01292.
- [7] J. Qian, X. Gao, and B. Pan. “Nanoconfinement-Mediated Water Treatment: From Fundamental to Application.” *Environmental Science & Technology* (2020). doi:10.1021/acs.est.0c01065.
- [8] S.-H. H. Chong and S. Ham. “Dynamics of Hydration Water Plays a Key Role in Determining the Binding Thermodynamics of Protein Complexes.” *Sci. Rep.*, 7(1):8744 (2017). doi:10.1038/s41598-017-09466-w.
- [9] M. K. Cho, S.-H. Chong, S. Shin, and S. Ham. “Site-Specific Backbone and Side-Chain Contributions to Thermodynamic Stabilizing Forces of the WW Domain.” *J. Phys. Chem. B*, 125(26):7108–7116 (2021). doi:10.1021/ACS.JPCB.1C01725.
- [10] M.-C. Bellissent-Funel, A. Hassanali, M. Havenith, R. Henchman, P. Pohl, F. Sterpone, D. van der Spoel, Y. Xu, and A. E. Garcia. “Water Determines the Structure and Dynamics of Proteins.” *Chem. Rev.*, 116(13):7673–7697 (2016). doi:10.1021/acs.chemrev.5b00664.
- [11] S. Cervený, F. Mallamace, J. Swenson, M. Vogel, and L. Xu. “Confined Water as Model of Supercooled Water.” *Chem. Rev.*, 116(13):7608–7625 (2016). doi:10.1021/acs.chemrev.5b00609.
- [12] R. Biswas and B. Bagchi. “Anomalous water dynamics at surfaces and interfaces: synergistic effects of confinement and surface interactions.” *J. Phys.: Condens. Matter*, 30(1):013001 (2018). doi:10.1088/1361-648X/aa9b1d.
- [13] H.-S. Tan, I. R. Piletic, R. E. Riter, N. E. Levinger, and M. D. Fayer. “Dynamics of Water Confined on a Nanometer Length Scale in Reverse Micelles: Ultrafast Infrared Vibrational Echo Spectroscopy.” *Phys. Rev. Lett.*, 94(5):057405 (2005). doi:10.1103/PhysRevLett.94.057405.
- [14] M. D. Fayer and N. E. Levinger. “Analysis of Water in Confined Geometries and at Interfaces.” *Annu. Rev. Anal. Chem.*, 3(1):89–107 (2010). PMID: 20636035. doi:10.1146/annurev-anchem-070109-103410.
- [15] B. P. Wiebenga-Sanford, J. B. Washington, B. Cosgrove, E. F. Palomares, D. A. Vasquez, C. D. Rithner, and N. E. Levinger. “Sweet Confinement: Glucose and Carbohydrate Osmolytes in Reverse Micelles.” *J. Phys. Chem. B*, 122(41):9555–9566 (2018). doi:10.1021/acs.jpcc.8b07406.
- [16] I. R. Piletic, D. E. Moilanen, D. B. Spry, N. E. Levinger, and M. D. Fayer. “Testing the Core/Shell Model of

- Nanoconfined Water in Reverse Micelles Using Linear and Nonlinear IR Spectroscopy.” *J. Phys. Chem. A*, 110(15):4985–4999 (2006). doi:10.1021/jp061065c.
- [17] M. R. Harpham, B. M. Ladanyi, N. E. Levinger, and K. W. Herwig. “Water motion in reverse micelles studied by quasielastic neutron scattering and molecular dynamics simulations.” *J. Chem. Phys.*, 121(16):7855 (2004). doi:10.1063/1.1792592.
- [18] N. Sarkar, K. Das, A. Datta, S. Das, and K. Bhattacharyya. “Solvation Dynamics of Coumarin 480 in Reverse Micelles. Slow Relaxation of Water Molecules.” *J. Phys. Chem.*, 100(25):10523–10527 (1996). doi:10.1021/jp953658l.
- [19] D. Singha, N. Barman, A. Phukon, and K. Sahu. “Selective Probing of Reverse Micelle Interfacial Layer upon Silver Nanoparticle Formation using Dynamic Stokes Shift Measurements.” *J. Phys. Chem. C*, 118(19):10366–10374 (2014). doi:10.1021/jp500029q.
- [20] J. Faeder and B. M. Ladanyi. “Solvation Dynamics in Reverse Micelles: The Role of Headgroup-Solute Interactions.” *J. Phys. Chem. B*, 109(14):6732–6740 (2005). doi:10.1021/jp045202m.
- [21] J. Lee, M. Maj, K. Kwak, and M. Cho. “Infrared Pump-Probe Study of Nanoconfined Water Structure in Reverse Micelle.” *J. Phys. Chem. Lett.*, 5(19):3404–3407 (2014). doi:10.1021/jz501737q.
- [22] V. P. Roy and K. J. Kubarych. “Interfacial Hydration Dynamics in Cationic Micelles Using 2D-IR and NMR.” *J. Phys. Chem. B*, 121(41):9621–9630 (2017). doi:10.1021/acs.jpcc.7b08225.
- [23] G. Carlstroem and B. Halle. “Shape fluctuations and water diffusion in microemulsion droplets: a nuclear spin relaxation study.” *J. Phys. Chem.*, 93(8):3287–3299 (1989). doi:10.1021/j100345a080.
- [24] G. Carlstroem and B. Halle. “Water dynamics in microemulsion droplets. A nuclear spin relaxation study.” *Langmuir*, 4(6):1346–1352 (1988). doi:10.1021/la00084a025.
- [25] P.-O. Quist and B. Halle. “Water dynamics and aggregate structure in reversed micelles at sub-zero temperatures. A deuteron spin relaxation study.” *J. Chem. Soc., Faraday Trans. 1 F*, 84(4):1033–1046 (1988). doi:10.1039/F19888401033.
- [26] M. D’Angelo, D. Fioretto, G. Onori, L. Palmieri, and A. Santucci. “Dynamics of water-containing sodium bis(2-ethylhexyl)sulfosuccinate (AOT) reverse micelles: A high-frequency dielectric study.” *Physical Review E*, 54(1):993–996 (1996). PMID: 9965156. doi:10.1103/PhysRevE.54.993.
- [27] Pan Tan, P. Tan, Juan Huang, J. Huang, Eugene Mamontov, E. Mamontov, Victoria García Sakai, V. G. Sakai, Franci Merzel, F. Merzel, Zhuo Liu, Z. Liu, Yiyang Ye, Y. Ye, Liang Hong, and L. Hong. “Decoupling between the translation and rotation of water in the proximity of a protein molecule.” *Phys. Chem. Chem. Phys.*, 22(32):18132–18140 (2020). PMID: 32761039. doi:10.1039/d0cp02416c.
- [28] G. Schirò, Y. Fichou, F.-X. Gallat, K. Wood, F. Gabel, M. Moulin, M. Härtlein, M. Heyden, J.-P. Colletier, A. Orecchini, A. Paciaroni, J. Wuttke, D. J. Tobias, and M. Weik. “Translational diffusion of hydration water correlates with functional motions in folded and intrinsically disordered proteins.” *Nat. Commun.*, 6(1):6490 (2015). doi:10.1038/ncomms7490.
- [29] G. Schirò and M. Weik. “Role of hydration water in the onset of protein structural dynamics.” *J. Phys.: Condens. Matter*, 31(46):463002 (2019). PMID: 31382251. doi:10.1088/1361-648X/AB388A.
- [30] R. Zhang, Y. Chen, D. Troya, and L. A. Madsen. “Relating Geometric Nanoconfinement and Local Molecular Environment to Diffusion in Ionic Polymer Membranes.” *Macromolecules*, 53(9):3296–3305 (2020). doi:10.1021/acs.macromol.9b02755.
- [31] J. M. Franck, Y. Ding, K. Stone, P. Z. Qin, and S. Han. “Anomalously Rapid Hydration Water Diffusion Dynamics Near DNA Surfaces.” *J. Am. Chem. Soc.*, 137(37):12013–12023 (2015). doi:10.1021/jacs.5b05813.
- [32] R. Barnes, S. Sun, Y. Fichou, F. W. Dahlquist, M. Heyden, and S. Han. “Spatially Heterogeneous Surface Water Diffusivity around Structured Protein Surfaces at Equilibrium.” *J. Am. Chem. Soc.*, 139(49):17890–17901 (2017). doi:10.1021/jacs.7b08606.
- [33] J. M. Franck and S. Han. “Overhauser Dynamic Nuclear Polarization for the Study of Hydration Dynamics, Explained.” In A. J. Wand, editor, “Biological NMR Part B,” volume 615 of *Methods in Enzymology*, pages 131–175. Academic Press (2019).
- [34] B. D. Armstrong, J. Choi, C. J. López, D. A. Wesener, W. Hubbell, S. Cavagnero, and S. Han. “Site-Specific Hydration Dynamics in the Nonpolar Core of a Molten Globule by Dynamic Nuclear Polarization of Water.” *J. Am. Chem. Soc.*, 133(15):5987–5995 (2011). doi:10.1021/ja111515s.
- [35] C.-Y. Cheng and S. Han. “Dynamic nuclear polarization methods in solids and solutions to explore membrane proteins and membrane systems.” *Ann Rev Phys Chem*, 64:507–32 (2013). PMID: 23331309. doi:10.1146/annurev-physchem-040412-110028.
- [36] T. Übrück, O. Neudert, K.-D. Kreuer, B. Blümich, J. Granwehr, S. Stapf, and S. Han. “Effect of nitroxide spin probes on the transport properties of Nafion membranes.” *Phys. Chem. Chem. Phys.*, 20(41):26660–26674 (2018). doi:10.1039/C8CP04607G.
- [37] H. Moon, R. P. Collanton, J. I. Monroe, T. M. Casey, M. S. Shell, S. Han, and S. L. Scott. “Evidence for Entropically Controlled Interfacial Hydration in Mesoporous Organosilicas.” *J. Am. Chem. Soc.*, 144(4):1766–1777 (2022). doi:10.1021/jacs.1c11342.
- [38] K. G. Valentine, G. Mathies, S. Bédard, N. V. Nucci, I. Dodevski, M. A. Stetz, T. V. Can, R. G. Griffin, and A. J. Wand. “Reverse Micelles As a Platform for Dynamic Nuclear Polarization in Solution NMR of Proteins.” *J. Am. Chem. Soc.*, 136(7):2800–2807 (2014). doi:10.1021/ja4107176.
- [39] G. Haering, P. L. Luisi, and H. Hauser. “Characterization by electron spin resonance of reversed micelles consisting of the ternary system AOT-isooctane-water.” *J. Phys. Chem.*, 92(12):3574–3581 (1988). doi:10.1021/j100323a050.
- [40] G. M. Clore and J. Iwahara. “Theory, Practice, and Applications of Paramagnetic Relaxation Enhancement for the Characterization of Transient Low-Population States of Biological Macromolecules and Their Complexes.” *Chem. Rev.*, 109(9):4108–4139 (2009). doi:10.1021/cr900033p.
- [41] H. Hauser, G. Haering, A. Pande, and P. L. Luisi. “Interaction of water with sodium bis(2-ethyl-1-hexyl)

- sulfosuccinate in reversed micelles.” *J. Phys. Chem.*, 93(23):7869–7876 (1989). doi:10.1021/j100360a029.
- [42] J. M. Franck, A. Pavlova, J. A. Scott, and S. Han. “Quantitative cw Overhauser effect dynamic nuclear polarization for the analysis of local water dynamics.” *Prog. Nucl. Magn. Reson. Spectrosc.*, 74:33–56 (2013). PMID: 24083461. doi:10.1016/j.pnmrs.2013.06.001.
- [43] D. E. Moilanen, E. E. Fenn, D. Wong, and M. D. Fayer. “Water dynamics in large and small reverse micelles: From two ensembles to collective behavior.” *J. Chem. Phys.*, 131(1) (2009). PMID: 19586114. doi:10.1063/1.3159779.
- [44] J. M. Franck, J. A. Scott, and S. Han. “Nonlinear Scaling of Surface Water Diffusion with Bulk Water Viscosity of Crowded Solutions.” *J. Am. Chem. Soc.*, 135(11):4175–4178 (2013). doi:10.1021/ja3112912.
- [45] N. Pal, S. D. Verma, M. K. Singh, and S. Sen. “Fluorescence Correlation Spectroscopy: An Efficient Tool for Measuring Size, Size-Distribution and Polydispersity of Microemulsion Droplets in Solution.” *Anal. Chem.*, 83(20):7736–7744 (2011). doi:10.1021/ac2012637.
- [46] J. M. Franck, M. Sokolovski, N. Kessler, E. Matalon, M. Gordon-Grossman, S.-i. Han, D. Goldfarb, and A. Horovitz. “Probing Water Density and Dynamics in the Chaperonin GroEL Cavity.” *J. Am. Chem. Soc.*, 136(26):9396–9403 (2014). doi:10.1021/ja503501x.
- [47] M. Ueda and Z. A. Schelly. “Mean aggregation number and water vapor pressure of AOT reverse micellar systems determined by controlled partial pressure-vapor pressure osmometry (CPP-VPO).” *Langmuir*, 4(3):653–655 (1988). doi:10.1021/la00081a026.
- [48] A. A. Beaton, A. Guinness, and J. M. Franck. “Rapidly Screening the Correlation Between the Rotational Mobility and the Hydrogen Bonding Strength of Confined Water.” (2023). Manuscript id: ac-2023-05769q
Manuscript id: ac-2023-05769q.

Supplemental Materials for: Direct Observation of the Translational Immobilization of Water Molecules Under Nanoscale Confinement

Please note that all figure/table/equation references that are not prefixed with “SI” refer to the main text.

SI. Theory and Data Analysis

A spin cross-relaxation (k_σ) transition is always active when an electron spin and water are present. This transition is excited by molecular motion that is sufficiently fast to cause high frequency fluctuations of the magnetic dipole-dipole coupling between the electron and proton (hydrogen nuclei of the water) spins. By saturating (strongly exciting) the Electron Spin Resonance (ESR) transition to push the spin states away from thermal equilibrium, Overhauser Dynamic Nuclear Polarization (ODNP) makes this cross-relaxation visible, specifically resulting in the enhancement and inversion of the nuclear (proton) spin states. By normalizing the enhancements against the Nuclear Magnetic Resonance (NMR) relaxation and driving the ESR transition to saturation, we can determine the transition rate of this cross-relaxation and relate it to the translational diffusion near the electron spin probe (SP) [1–3].

Thus, cross-relaxivity, k_σ (units $\text{s}^{-1}\text{M}^{-1}$, rate per SP concentration), measures fluctuations in local magnetic fields generated by the translational motion of water. ODNP also offers a measurement of the low-frequency relaxivity, k_{low} , that senses motion on a slower timescale, such as proton exchange or, here, tumbling of the reverse micelle [1, 3]. The quantification of both k_σ and k_{low} relies on measurements of the the integrated signal intensity $I(p)$ as a function of microwave power, p . The $I(p)$ are typically normalized by the signal in the absence of microwave power $I(0)$ to give the ODNP signal enhancements $E(p) = I(p)/I(0)$. The $E(p)$ relate to the cross-relaxivity k_σ discussed in the main text by way

of [3]:

$$1 - E(p) = \underbrace{T_1(p)k_\sigma s(p)C_{SL}}_{1/\text{rate of thermal relaxation}} \overbrace{\left| \frac{\omega_e}{\omega_H} \right|}^{\text{rate of hyperpolarization}}, \quad (\text{S1})$$

As indicated by the standard protocol [3], inversion-recovery measurements of the NMR relaxation times $T_1(p)$ at 3–5 select microwave powers, p , are interpolated, allowing division of $1 - E(p)$ by $C_{SL} |\omega_e/\omega_H| T_1(p)$, where $|\omega_e/\omega_H|$ is a constant (659.3), and C_{SL} gives the number of moles of SP per liter of aqueous solution (here $C_{SL} = 70$ mM for all samples). This division accomplishes the transformation from Fig. 2a to Fig. 2b. Fig. 2b displays $k_\sigma s(p)$; *i.e.*, it depends on the saturation of the ESR transition, $s(p)$, in addition to the desired cross-relaxivity. Therefore, as noted in the text, $s(p)$ is fit to:

$$s(p) = \frac{s_{max}}{p + p_{1/2}} \quad (\text{S2})$$

where $p_{1/2}$ is a fitting parameter that depends on the characteristics of the hardware, while s_{max} indicates the maximal electron spin saturation. Here, it is reasonable [4–6] to assume that the slow tumbling seen in Fig. S3 drives s_{max} to 1 by way of a ^{14}N relaxation mechanism that mixes the saturation of the 3 hyperfine lines.

The value of k_{low} can be determined by subtracting the fast-motional k_σ from the self-relaxivity [3], k_ρ :

$$k_{low} = \frac{5}{3}k_\rho - \frac{7}{3}k_\sigma \quad (\text{S3})$$

where k_ρ is defined as

$$k_\rho = \frac{T_1^{-1}(0) - T_{1,0}^{-1}(0)}{C_{SL}} \quad (\text{S4})$$

where $T_1(0)$ is the T_1 relaxation time of the sample in consideration with a SP concentration of C_{SL} at no microwave power ($p = 0$) and $T_{1,0}(0)$ is the T_1 relaxation time of this same sample without any SP present (also at $p = 0$). The unitless parameters $\left(\frac{k_\sigma}{k_{\sigma,bulk}}\right)^{-1}$ and $\left(\frac{k_{low}}{k_{low,bulk}}\right)$ enable facile comparison to existing ODNP measurements in the literature, as described in [2, 3]. The bulk values of $k_\sigma = 95.4 \text{ M}^{-1}\text{s}^{-1}$ and $k_{low} = 366 \text{ M}^{-1}\text{s}^{-1}$ are used to complete this analysis [7].

High-field (400 MHz) ^1H Paramagnetic Relaxation Enhancement (PRE)-Relaxation-Ordered Spectroscopy (ROSY) measurements identify the location of the small-molecule SPs in this study. PRE is a well-established NMR technique in which the presence of nearby SPs causes nearby nuclei to relax more rapidly than they would in the absence of the SP [8]. In this way, PRE can be used to obtain distance information in, *e.g.* biological systems, where a covalently linked SP can be used to report on nuclei near that SP. (Or where small molecule SP in solution helps to identify surface-exposed sites.)

As with ODNP, PRE is brought about by dipolar interaction between an electron spin and a nuclear spin. Typically, for a SP with $S = 1/2$, like a nitroxide, this takes the form [8]:

$$R_1 - R_{1,0} = \frac{1}{T_1} - \frac{1}{T_{1,0}} = \frac{3}{10} \left(\frac{\mu_0}{4\pi}\right)^2 \frac{\hbar^2 \gamma_I^2 \gamma_S^2}{r^6} \frac{\tau_c}{1 + (\omega\tau_c)^2} \quad (\text{S5})$$

where T_1 and $T_{1,0}$ are the NMR relaxation times (and R_1 and $R_{1,0}$ the corresponding rates) with and without the spin label (here at high field and resonance frequency), γ_I and γ_S are the gyromagnetic ratios of the nuclear spin and electron spin, respectively, r is the distance between the spins, ω is the resonance frequency (here $2\pi \times 400 \text{ MHz}$) and τ_c the correlation time of the relative motion of the spin probe and molecule of interest, under the assumption that the electron spin relaxes too quickly to be affected by motion on this timescale [9, 10]. Note that, for very fast motions, $\omega\tau_c$ will approach zero.

Of note in Eq. (S5) is the squared dependence on γ_S , making the relaxation arising from coupling to electron spins many orders of magnitude faster than that arising from other nuclear spins. As such, dipolar relaxation in the presence of unpaired electrons tends to dominate all other relaxation mechanisms in proton NMR, where its contribution to $R_1 = 1/T_1$ is very large. Also of note, the γ_I^2 dependence of Eq. (S5) suppresses the PRE effect for low- γ nuclei. Since γ_I is $6.5\times$ smaller for ^2H than it is for ^1H , and, furthermore, for ^2H , a quadrupolar mechanism drives a relatively large contribution to the $1/T_1$ rate, the PRE contributes negligibly in deuterium NMR [11].

In this study, because both the spin probe and the molecules experiencing PRE are relatively small in size (compared to *e.g.* proteins that are also studied by PRE), it is important to note that Eq. (S5) scales with $1/r^6$, so close-contact interactions will tend to dominate the PRE

interaction. The PRE in this context can be said to be a measure of how often a given molecule or group comes close to the SP.

S1.1. Size of reverse micelles (RMs)

Various points in the manuscript reference the number of waters present inside the RM. While there are various schemes for estimating this number, as noted in [12], we employ a meta-analysis of several sources [13–16] to arrive at the equation for the number of AOT molecules (aggregation number \bar{n}) per RM:

$$\exp(k\bar{n}) = \exp(ka) + \exp(k(mw_0 + b)) + \exp(k(lw_0^2 + c)) \quad (\text{S6})$$

From \bar{n} , one can in turn determine the number of water molecules, $\bar{n}w_0$, at a given water loading. In Eq. (S6), the value of $a = 15.1$ gives number of AOT molecules in the constant- \bar{n} regime, the value of $m = 7.15$ gives the slope of the linear region (number of AOT molecules added per change in w_0), $b = 0.259$ the intercept of the linear regime, $l = 0.673$ the curvature of the quadratic regime, $c = -37.1$ the intercept of the quadratic equation, and the value of $k = 0.174$ gives the curvature between the constant, linear, and quadratic regimes.

S2. Experimental

S2.1. Sample preparation

Two SPs were studied in this work: TEMPOL (4-hydroxy-2,2,6,6-tetramethylpiperidin-1-oxyl), and the ionic TEMPO-SO₄ (4-sulfate-2,2,6,6-tetramethylpiperidin-1-oxyl potassium salt), as shown on the left side of Fig. 1. The nitroxide moiety is located on a neutral, polar molecule in TEMPOL and on a negatively charged ion in TEMPO-SO₄.

TEMPO-SO₄ was synthesized using a previously described procedure [17]. The lowest and highest w_0 RMs were prepared first, and intermediate w_0 samples were prepared by mixing appropriate aliquots from each in order to keep the concentration of Aerosol-OT (AOT) constant across all sample preparations. The constant AOT concentration (as opposed to a constant water concentration) in all samples better suits the ability to background subtract contributions to the NMR signal.

The lowest water loading sample ($w_0 = 1$) was prepared by adding AOT (4.37 g, 0.00983 mol) to 6.765 mL (10.78 g) CCl₄. The clear solution was vortexed until all AOT was dissolved, after which 179 μL of 70 mM TEMPO-SO₄ was added to the solution and vortexed 30 seconds $3\times$. The highest water loading sample ($w_0 = 10$) was prepared by adding AOT (4.44 g, 0.00999 mol) to 6.765 mL CCl₄ and dissolving completely, after which 1800 μL of 70 mM TEMPO-SO₄ was added to the solution and vortexed for 30 seconds $3\times$. After vortexing, each sample was capped, wrapped in parafilm, placed in a desiccator, and allowed to sit at room temperature for several hours. The final solutions had a slight red color (arising from the nitroxide), most noticeable in the $w_0 = 10$ sample. These preparations correspond to mass

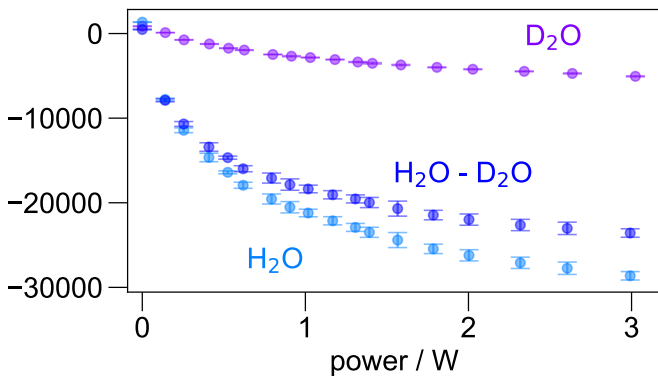


FIG. S1. The unnormalized signal intensity curves for $w_0 = 10$ AOT/ CCl_4 RMs, showing the difference between a sample prepared with H_2O vs D_2O . The D_2O data contains only enhanced signal from the surfactant. The units of the y -axis are arbitrary units for the integrated NMR signal intensity. The subtraction is performed on the unnormalized data and also shown; the subtracted data is subsequently normalized by the value at $p = 0$ to generate the appropriate $E(p)$ curve.

percentages of 63%, 29%, and 11% for the $w_0 = 10$ sample and 70%, 29%, and 1% for the $w_0 = 1$ sample for CCl_4 , AOT, and water, respectively. Given that these samples were prepared in CCl_4 , the highest w_0 attainable is around 10 [18].

To prepare the $w_0 = 5$ sample, 2070 μL of each the $w_0 = 1$ and $w_0 = 10$ samples were combined to give a final solution volume of 4140 μL ; to prepare the $w_0 = 7$ sample, 1320 μL of each the $w_0 = 5$ and 10 samples were combined to give a final solution volume of 2640 μL ; *etc.* These solutions were vortexed for 30 seconds $3\times$ and allowed to become fully transparent before mixing subsequent aliquots or preparing NMR samples. After attaining full transparency, each sample exhibited a slight red color as with the initial $w_0 = 10$ solution.

To prepare the parallel D_2O samples, the same preparation was followed with equivalent amounts of a 70 mM TEMPO- SO_4 D_2O solution used in place of the H_2O solution. The parallel D_2O samples provide background signal to account for any enhancement of the AOT protons that contribute to the detected signal, as in the work by Valentine and coworkers [19], and as shown in Fig. S1.

S2.2. ODNP measurements

ODNP measurements were performed on a system comprising a home-built NMR probe that inserts into a Bruker Super High Sensitivity Probehead X-Band resonator (ER 4122 SHQE, probe as in [5]), of a Bruker E500 cw EPR, a home-built receiver box (with home-built duplexer, Minicircuits ZFL-500LN+, and various commercial filters), a SpinCore RadioProcessor-G transceiver board to digitize the signal, and a Bridge12 Microwave Power Source (MPS).

The field concomitant with the lowest field hyperfine line (see Fig. S3) was used as the B_0 field for ODNP measurements. The exact field position was determined be-

fore each ODNP experiment by performing a field sweep of the NMR resonance with 3 W of incident microwave power, thus identifying the field position at which maximum enhancement occurs (approximately 3490 G for a microwave frequency of 9.8 GHz).

The python extension for controlling the SpinCore transceiver with a simple list-based pulse program format and automating the ODNP experiments is available at https://github.com/jmfrancklab/spincore_apps this relies in part on the library available at https://github.com/jmfrancklab/inst_notebooks, which provides utilities for interfacing with the MPS (to control the microwave power) as well as the Bruker magnet (to change the field), and provides continuous logging of the microwave power incident on the sample. All data is stored in the standard HDF5 (Hierarchical Data Format) format.

Additional tools available in https://github.com/jmfrancklab/proc_scripts help to process signal following the procedure outlined in [20]. All the home-built libraries mentioned here utilize the pySpecData (<https://github.com/jmfrancklab/pyspecdata>) library, as it simplifies and clarifies all key tasks related to manipulating multi-dimensional spectroscopic data.

S2.3. PRE-ROSY measurements

PRE measurements were acquired with a custom inversion-recovery sequence on an Avance III HD 400 MHz. The variable delay list (for recovery delay τ) had roughly logarithmically spaced points, to capture both faster and slower relaxing components. Both to improve the signal-to-noise, and because the J -coupling multiplets of the surfactant appear different for different levels of T_1 relaxation, the spectral dimension is subjected to significant Gaussian apodization (0.05 ppm). The R_1 distributions were implemented by following a 1D version of the Inverse Laplace Transform (ILT) outlined in [21], in particular utilizing the compressed implementation of the BRD [22] method for choosing the regularization parameter. The algorithm is available as part of the pySpecData library (`nnls` function). For the PRE data, a basis of linearly spaced $R_1 = 1/T_1$ values was chosen, with kernel $K(R_1, \tau) = \exp(-R_1\tau)$. Samples for PRE-ROSY followed the same general scheme as noted above, except that trace amounts of tetramethylsilane (TMS) were added to the sample.

S2.4. Further notes on determination of k_{low}

Note that to determine k_{low} , a non-ODNP-enhanced NMR experiment must measure the relaxation rate in the absence of SP. As this measurement involves a prohibitively low level of signal-to-noise ratio (SNR), it was only performed for the highest w_0 RM, where water is expected to have the longest relaxation time. Thus, Table I indicates the lower bound for k_{low} in all cases.

S3. Further notes on PRE-ROSY

In Fig. 1, it is worth noting that the surfactant peaks experience slightly less PRE from the TEMPO- SO_4 *vs.*

TEMPOL that becomes more apparent upon zooming in on the relevant peaks. This is consistent with the general result that the TEMPO-SO₄ remains better localized to the middle of the water pool, away from both dispersant and surfactant.

It is also worth noting that at any instant, multiple different populations of RM coexist in equilibrium: one of RMs loaded with a single SP, another with no SP, a third with two SPs, *etc.*. The exchange of water from one RM to another should be relatively slow. Each population of RMs with different numbers of encapsulated SPs provides a different micro-environment for the water, which will relax more rapidly inside RMs with more SPs. The ROSY spectrum, however, shows only one peak in the T_1 distribution, indicating that the slow exchange of water between the different RM microenvironments still occurs on a timescale that is faster than the T_1 of the (SP-labeled) RM – *i.e.*, faster than about 100 ms. Therefore, the ROSY results also highlight that measurements of ODNP cross-relaxation (k_σ) will be averaged across all RMs in the ensemble.

S4. ²H ROSY to check for structural perturbation of Water

As an important control, the deuterium relaxometry screening technique (Automated Deuterium Relaxation-Ordered Spectroscopy in Solution (ADROSYS)) described in [12] was applied to study the TEMPO-SO₄ loaded RM system, to check whether the SP might be significantly perturbing the properties of the confined water. In this way, the SP acts like the inclusion molecules studied in [12]. This technique could offer insight into any changes to the hydrogen bonding strength or rotational mobility of water in this RM system. Importantly, unlike ¹H nuclei, however, ²H nuclei do not experience a dramatic PRE effect in the presence of unpaired electrons [11] (due to the γ_I^2 scaling in Eq. (S5)). As a consequence, the resulting relaxometry data should not reflect much of a change relative to the “empty” (water-only) RM system.

Fig. 2b presents data for TEMPO-SO₄ loaded RMs with sample preparations ranging from $w_0 = 1.0$ to 8.1. The expected behavior is observed – namely, that there is an increase in ²H T_1 and chemical shift as w_0 increases. When compared to the data of Fig. 2a in [12], from RMs of similar sizes in the same dispersant (CCl₄) but without any SP, there is general agreement. One slight difference is that upon incorporation of the SP (compare Fig. 2a *vs.* Fig. 2b), the distribution for the $w_0 = 1$ broadens somewhat. This is consistent with the data obtained in the presence of guest molecules present in high concentrations, such as the glucose and PEG-200 data reported in [12], and could indicate a change in the size distribution of the RMs resulting from inclusion of the guest molecule. The slight change in chemical shift seen for all water loadings (compare Fig. 2a *vs.* Fig. 2b), is likely consistent with a paramagnetic shift upon incorporation of the SP. Overall, this data thus indicate that the SP does not dramatically perturb the rotational motion or

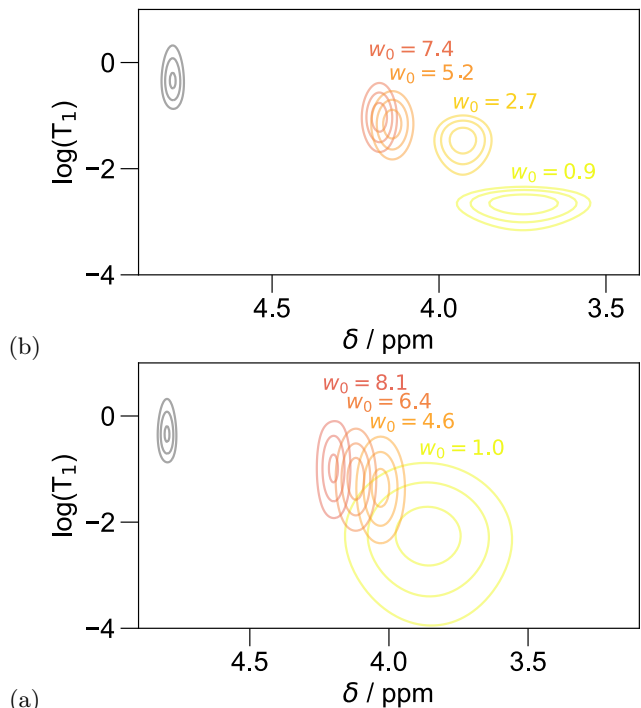


FIG. S2. ILT plot showing the T_1 of D₂O for different AOT RMs prepared in CCl₄ (a) and in CCl₄ with added spin probe TEMPO-SO₄ (b) for water loadings ranging from 1 to 8.

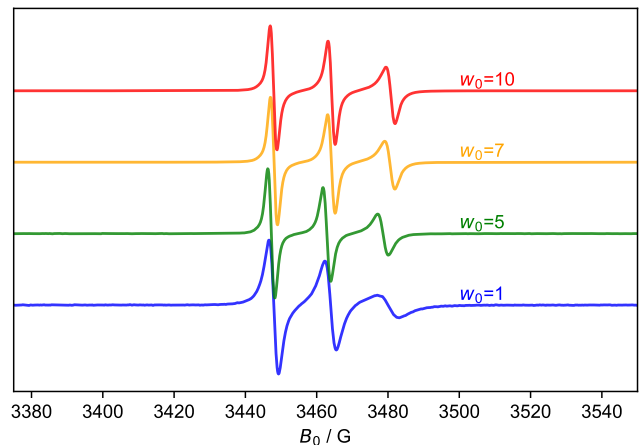


FIG. S3. Normalized ESR spectra acquired for the RM samples containing TEMPO-SO₄ in H₂O for $w_0 = 1$ (blue), 5 (orange), 7.6 (green), and 10 (red).

hydrogen bonding network of the internal water pool at the concentration (70 mM) used.

S4.1. Electron Spin Resonance

The RM samples were also analyzed by cw ESR at 9.8 GHz in Fig. S3. In line with previous measurements [23, 24], the ESR spectra show a restriction of the SP mobility at the lowest water loadings ($w_0 = 1$, blue) and an incremental increase in the mobility as the w_0 increases, up to the highest w_0 in these measure-

w_0	τ_c/ns
1	1.7
5	0.51
7	0.44
10	0.35

TABLE I. ESR correlation times corresponding to the spectra in Fig. S3.

ments ($w_0 = 10$, red). Specifically, the ESR spectra for nitroxide SPs inside RMs exhibit a characteristic decrease in intensity of the three hyperfine lines from lowest to highest field (left to right) as well as a general broadening of all lines due to the reduced rotational correlation time of the SP. (Note that ESR spectra are presented as a derivative of the absorption spectra, so that each positive-negative pair in the lineshape is referred to as a “line.”) The difference from nitroxides freely dissolved in either water or organic solvent at room temperature, which present three roughly equal lines, is consistent with the fact that at all w_0 studied here, RMs were successfully formed and the SP remained trapped inside the aqueous core of the RM. The equation [25]

$$\tau_c = (6.51 \times 10^{-10} \text{ s}) \left(\frac{\Delta H_0}{\text{G}} \right) \left(\sqrt{\frac{h(0)}{h(-1)}} + \sqrt{\frac{h(0)}{h(+1)}} - 2 \right)$$

approximates the rotational correlation times, where s and G are units (seconds and Gauss); $h(+1)$, $h(0)$, and $h(-1)$ are the peak-to-peak amplitudes of the ESR lines;

and ΔH_0 is the peak-to-peak linewidth of the central line.

The trend observed is opposite what one would expect from a Stoke-Debye-Einstein prediction of the rotational correlation time of the RM (*i.e.*, $\tau_R \propto R^{-3}$ with R the RM radius). Rather, the decreasing correlation time with increasing RM diameter is consistent with the notion that the water pool develops more bulk-like character with increasing w_0 and that the microviscosity decreases with increasing w_0 . Similar results have been observed previously for slightly different SPs [25], and prove consistent with (though less direct than) the ODNP results presented here. Notably, the spectrum for the highest w_0 studied here ($w_0 = 10$) still does not exhibit hyperfine lines of equal intensity, as expected for a SP free in solution, thus indicating that there is still some amount of rotational retardation. However, for small w_0 , as the water becomes very viscous and potentially almost completely immobilizes the SP relative to the reverse micelle, the τ_c observed in the ESR spectrum will report almost exclusively on the rotational correlation time of the water.

S5. Other methods of extrapolation

Extrapolating a quadratic fit of the k_σ vs. the water pool diameter indicates a water pool diameter of 6.7 nm is needed which is roughly $w_0 = 20$: although not quite as large, this gain confirms that a very large assembly of water molecules is needed to provide bulk-like translational dynamics.

-
- [1] J. M. Franck, Y. Ding, K. Stone, P. Z. Qin, and S. Han. “Anomalous Rapid Hydration Water Diffusion Dynamics Near DNA Surfaces.” *J. Am. Chem. Soc.*, 137(37):12013–12023 (2015). doi:10.1021/jacs.5b05813.
- [2] R. Barnes, S. Sun, Y. Fichou, F. W. Dahlquist, M. Heyden, and S. Han. “Spatially Heterogeneous Surface Water Diffusivity around Structured Protein Surfaces at Equilibrium.” *J. Am. Chem. Soc.*, 139(49):17890–17901 (2017). doi:10.1021/jacs.7b08606.
- [3] J. M. Franck and S. Han. “Overhauser Dynamic Nuclear Polarization for the Study of Hydration Dynamics, Explained.” In A. J. Wand, editor, “Biological NMR Part B,” volume 615 of *Methods in Enzymology*, pages 131–175. Academic Press (2019).
- [4] B. D. Armstrong, J. Choi, C. J. López, D. A. Wesener, W. Hubbell, S. Cavagnero, and S. Han. “Site-Specific Hydration Dynamics in the Nonpolar Core of a Molten Globule by Dynamic Nuclear Polarization of Water.” *J. Am. Chem. Soc.*, 133(15):5987–5995 (2011). doi:10.1021/ja111515s.
- [5] J. M. Franck, A. Pavlova, J. A. Scott, and S. Han. “Quantitative cw Overhauser effect dynamic nuclear polarization for the analysis of local water dynamics.” *Prog. Nucl. Magn. Reson. Spectrosc.*, 74:33–56 (2013). PMID: 24083461. doi:10.1016/j.pnmrs.2013.06.001.
- [6] B. Robinson, D. Haas, and C. Mailer. “Molecular dynamics in liquids: Spin-lattice relaxation of nitroxide spin labels.” *Science*, 263(5146):490–493 (1994). doi:10.1126/science.8290958.
- [7] J. M. Franck, M. Sokolovski, N. Kessler, E. Mat-alon, M. Gordon-Grossman, S.-i. Han, D. Goldfarb, and A. Horovitz. “Probing Water Density and Dynamics in the Chaperonin GroEL Cavity.” *J. Am. Chem. Soc.*, 136(26):9396–9403 (2014). doi:10.1021/ja503501x.
- [8] G. M. Clore and J. Iwahara. “Theory, Practice, and Applications of Paramagnetic Relaxation Enhancement for the Characterization of Transient Low-Population States of Biological Macromolecules and Their Complexes.” *Chem. Rev.*, 109(9):4108–4139 (2009). doi:10.1021/cr900033p.
- [9] N. Bloembergen, E. M. Purcell, and R. V. Pound. “Relaxation Effects in Nuclear Magnetic Resonance Absorption.” *Phys. Rev.*, 73(7):679–712 (1948). doi:10.1103/PhysRev.73.679.
- [10] I. Solomon. “Relaxation Processes in a System of Two Spins.” *Phys. Rev.*, 99(2):559–565 (1955). doi:10.1103/PhysRev.99.559.
- [11] H. H. Mantsch, H. Saitō, and I. C. P. Smith. “Deuterium magnetic resonance, applications in chemistry, physics and biology.” *Prog. Nucl. Magn. Reson. Spectrosc.*, 11(4):211–272 (1977). doi:10.1016/0079-6565(77)80010-1.
- [12] A. A. Beaton, A. Guinness, and J. M. Franck. “Rapidly Screening the Correlation Between the Rotational Mo-

- bility and the Hydrogen Bonding Strength of Confined Water.” *arXiv:2306.06571*, (arXiv:2306.06571) (2023).
- [13] M. Ueda and Z. A. Schelly. “Mean aggregation number and water vapor pressure of AOT reverse micellar systems determined by controlled partial pressure-vapor pressure osmometry (CPP-VPO).” *Langmuir*, 4(3):653–655 (1988). doi:10.1021/la00081a026.
- [14] G. Eskici and P. H. Axelsen. “The Size of AOT Reverse Micelles.” *J. Phys. Chem. B*, 120(44):11337–11347 (2016). doi:10.1021/ACS.JPCB.6B06420.
- [15] A. Amararene, M. Gindre, J.-Y. Le Huérou, W. Urbach, D. Valdez, and M. Waks. “Adiabatic compressibility of AOT [sodium bis(2-ethylhexyl)sulfosuccinate] reverse micelles: Analysis of a simple model based on micellar size and volumetric measurements.” *Phys. Rev. E*, 61(1):682–689 (2000). doi:10.1103/PhysRevE.61.682.
- [16] H.-F. Eicke and J. Rehak. “On the Formation of Water/Oil-Microemulsions.” *Helv. Chim. Acta*, 59(8):2883–2891 (1976). doi:10.1002/hlca.19760590825.
- [17] J. Winsberg, C. Stolze, A. Schwenke, S. Muench, M. D. Hager, and U. S. Schubert. “Aqueous 2,2,6,6-Tetramethylpiperidine-N-oxyl Catholytes for a High-Capacity and High Current Density Oxygen-Insensitive Hybrid-Flow Battery.” *ACS Energy Letters*, 2(2):411–416 (2017). doi:10.1021/acseenergylett.6b00655.
- [18] E. E. Fenn, D. B. Wong, and M. D. Fayer. “Water dynamics in small reverse micelles in two solvents: Two-dimensional infrared vibrational echoes with two-dimensional background subtraction.” *J. Chem. Phys.*, 134(5):054512 (2011). doi:10.1063/1.3532542.
- [19] K. G. Valentine, G. Mathies, S. Bédard, N. V. Nucci, I. Dodevski, M. A. Stetz, T. V. Can, R. G. Griffin, and A. J. Wand. “Reverse Micelles As a Platform for Dynamic Nuclear Polarization in Solution NMR of Proteins.” *J. Am. Chem. Soc.*, 136(7):2800–2807 (2014). doi:10.1021/ja4107176.
- [20] A. A. Beaton, A. Guinness, and J. M. Franck. “A modernized view of coherence pathways applied to magnetic resonance experiments in unstable, inhomogeneous fields.” *J. Chem. Phys.*, 157(17):174204 (2022). doi:10.1063/5.0105388.
- [21] L. Venkataramanan, Y. Q. Song, and M. D. Hürlimann. “Solving Fredholm integrals of the first kind with tensor product structure in 2 and 2.5 dimensions.” *IEEE Trans. Signal Process.*, 50(5):1017–1026 (2002). doi:10.1109/78.995059.
- [22] J. P. Butler, J. A. Reeds, and S. V. Dawson. “Estimating Solutions of First Kind Integral Equations with Nonnegative Constraints and Optimal Smoothing.” *SIAM J. Numer. Anal.*, 18(3):381–397 (1981). doi:10.1137/0718025.
- [23] G. Haering, P. L. Luisi, and H. Hauser. “Characterization by electron spin resonance of reversed micelles consisting of the ternary system AOT-isooctane-water.” *J. Phys. Chem.*, 92(12):3574–3581 (1988). doi:10.1021/j100323a050.
- [24] H. Hauser, G. Haering, A. Pande, and P. L. Luisi. “Interaction of water with sodium bis(2-ethyl-1-hexyl)sulfosuccinate in reversed micelles.” *J. Phys. Chem.*, 93(23):7869–7876 (1989). doi:10.1021/j100360a029.
- [25] H. Caldararu, A. Caragheorghopol, M. Vasilescu, I. Dragutan, and H. Lemmetyinen. “Structure of the Polar Core in Reverse Micelles of Nonionic Poly(oxyethylene) Surfactants, As Studied by Spin Probe and Fluorescence Probe Techniques.” *J. Phys. Chem.*, 98(20):5320–5331 (1994). doi:10.1021/j100071a024.